



Enhancement of H₂O₂ decomposition efficiency by the co-catalytic effect of iron phosphide on the Fenton reaction for the degradation of methylene blue

Can Ma^a, Shuo Feng^a, Jinming Zhou^a, Rufen Chen^a, Yu Wei^a, Hui Liu^{a,*}, Sen Wang^{b,**}

^a School of Chemistry and Material Science, Key Laboratory of Inorganic Nanomaterials of Hebei Province, National Demonstration Center for Experimental Chemistry Education Hebei Normal University, Shijiazhuang, 050024, China

^b Institute of Coal Chemistry, Chinese Academy of Sciences, Taiyuan, 030001, China



ARTICLE INFO

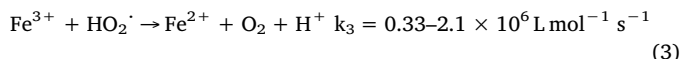
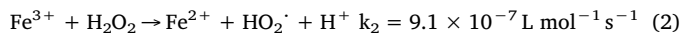
Keywords:
FeP/Fe^{II}
Co-catalyst
Heterogeneous Fenton
Methylene blue
Electron transfer

ABSTRACT

The greatest problem in the homogeneous Fenton reaction is the low production of HO· owing to the slow Fe^{III}/Fe^{II} cycle. In this study, we demonstrate a new co-catalyst of FeP and trace Fe²⁺ that can greatly enhance the decomposition efficiency of H₂O₂ and accelerate the degradation of methylene blue (MB). This co-catalyst is applicable in a broad pH range (pH = 3.0–9.0) and capable of degrading 95.74% and 89.01% of MB with 100 ppm in concentration within 30 s at pH 3 and 5, and 99.65% and 90.06% within 3 min at pH 7 and 9. The coexistence of FeP with Fe^{II} accelerates the Fe^{III}/Fe^{II} cycle by electron transfer between Fe⁸⁺ in FeP and Fe^{III}. Mössbauer spectra and density functional theory calculations indicate that the unique structure of FeP plays an important role in accelerating the Fe^{III}/Fe^{II} cycle.

1. Introduction

Advanced oxidation processes (AOPs) are considered promising strategies to remove organic pollutants from water. As a typical AOP, the homogeneous Fenton system (Fe²⁺/H₂O₂) is an efficient approach that can generate hydroxyl radicals (HO·) and address growing concerns toward the serious environmental pollution [1]. In the homogeneous Fenton system, three main reactions are involved (Eqs. 1–3) [2].



Here, Eq. 2 is the rate-limiting step leading to the low decomposition efficiency of H₂O₂ and a slow Fe^{III}/Fe^{II} cycle [3,4]. Due to the low solubility of the ferrous and ferric ions at high pH, the classic Fenton reaction has efficient reactivity only within a low and narrow pH range (pH 2.5–3.5), and problems associated with the precipitation of large amounts of Fe³⁺ sludge remarkably limit its practical applications [5–7]. To overcome these limitations, heterogeneous Fenton catalysts, zero-valent iron and iron oxides for instance, have been developed

[8,9]. Comparatively, these heterogeneous Fenton systems have proven to be promising alternatives because of its easy separation, which is favorable for practical applications. However, most of them still require lower pH values (3–5) and displayed relatively inert catalytic activity at higher pH values [10,11]. The low catalytic performance is because the heterogeneous Fenton reaction primarily catalyzes HO· evolution via Fe³⁺–H₂O₂ interactions, leading to slower HO· production rates [12]. A Fe^{III}/Fe^{II} redox cycle is also the core mechanism of heterogeneous Fenton chemistry; here, the reduction of structural Fe^{III} (\equiv Fe^{III}) to structural Fe^{II} (\equiv Fe^{II}) is the rate-limiting step responsible for the overall slow kinetics (Eqs. 4 and 5) [13].



Therefore, the key issue to accelerate the reaction rate from Fe^{III} to Fe^{II} becomes important to further improve the yielding efficiency of HO· in the heterogeneous Fenton system.

In this aspect, various iron-containing heterogeneous Fenton catalysts such as FeOCl, FeVO₄ and CuFeO₂ were developed [5,13–20]. Among them, FeOCl is an excellent example. The unique structural configuration of iron atoms in FeOCl facilitated rapid conversion of Fe^{III} to Fe^{II} [5,13]. Interestingly, the valence state of Fe^{III} in the FeOCl nanosheets decreases with decreasing thickness, which is beneficial for

* Corresponding author.

** Corresponding author.

E-mail addresses: liuhuicn@126.com (H. Liu), wangsen@sxicc.ac.cn (S. Wang).

the electron/charge transfer and the generation of HO[·] radicals [14]. The formation of FeOCl/POM heterojunctions also accelerated the reduction of Fe^{III} to Fe^{II} by improving the electron transfer from POMs to FeOCl [15].

In theory, co-catalysts could be more efficient than single component catalyst by utilizing the full potentials of each component. A combination of Fe@Fe₂O₃ and Fe²⁺ offered a superior Fenton catalyst to decompose H₂O₂ and produce HO[·] [21]. The anthraquinone-resin hybrid as a co-catalyst of Fenton-like reaction could accelerate the regeneration of Fe²⁺ ions through a quinone cycle under visible-light irradiation [22]. The inorganic co-catalysts WS₂ [2] and MoS₂ [23] of Fe^{II}/H₂O₂ Fenton system were also reported. The exposed reductive W⁴⁺ and Mo⁴⁺ on the surface of WS₂ and MoS₂ could greatly accelerate the rate-limiting step of Fe^{III}/Fe^{II} conversion, leading to rapid reduction of Cr(VI), remediation of phenol as well as inactivation of *Escherichia coli* K-12 and *Staphylococcus aureus*. In TiO₂/schwertmannite co-catalysis system, the photo-generated electrons from TiO₂ could continuously migrate to schwertmannite, which then could enhance the separation of electron-hole pairs on TiO₂ and accelerate the reduction of Fe^{III} to Fe^{II} on schwertmannite [24]. Despite of these interesting co-catalysts, to develop more effective co-catalysts are still of high necessity.

FeP is structurally different from other Fe-based catalysts such as FeOCl, FeVO₄, Fe₂O₃ and FeOOH etc. Fe in FeP is highly similar to metallic Fe but carries partial positive charges (Fe^{δ+}, 0 < δ+ < 2) and P in FeP carries partial negative charges (P^{δ-}, -1 < δ- < 0) [25–27]. Importantly, the P may form graphene-like networks with excellent electron conductivity [28], and this type of internal conduction may affect the rates of interfacial catalytic reactions [29]. We thus speculate that FeP, as a co-catalyst for Fe^{II}/H₂O₂ Fenton system, may accelerate the Fe^{III}/Fe^{II} conversion by electron transfer between Fe^{δ+} and Fe^{III} and improve the HO[·] yielding efficiency.

Herein, FeP nanoparticles are prepared by using β-FeOOH as precursor followed by reaction of β-FeOOH with NaH₂PO₂ in a N₂ atmosphere. FeP and trace Fe²⁺ (FeP/Fe^{II}) as co-catalyst was used to decompose H₂O₂ and degrade methylene blue (MB) for the first time. The co-catalyst exhibited excellent Fenton-like activity and high H₂O₂ utilization efficiency for the degradation of pollutants in a wide pH range. Fe^{II} adsorbed on FeP triggered the conversion from Fe^{II} to ≡Fe^{III} and FeP accelerated the conversion from ≡Fe^{III} to ≡Fe^{II} by electron transfer between Fe^{δ+} and ≡Fe^{III}. Mössbauer spectra and density functional theory (DFT) calculation confirmed that the electron transfer occurs within FeP. A novel catalytic mechanism for the co-catalytic Fenton-like reaction has been proposed. Moreover, FeP exhibits stable and recyclable co-catalytic performance for the Fe^{II}/H₂O₂ Fenton system, favoring the practical applications in pollutant removal.

2. Experimental sections

2.1. Materials

FeCl₃, NaOH, HCl and NaH₂PO₂ were purchased from Tianjin Yongda Chemical Corp. Hydrogen peroxide (H₂O₂, 30 wt%) were purchased from Tianjin Hengxing Chemical Corp. Titanium potassium oxalate (C₄K₂O₉Ti2H₂O) were purchased from Shanghai Macklin Biochemical Co., Ltd. Methylene blue was purchased from Aladdin Ltd. (Shanghai, China). All chemicals were used as received without further purification.

2.2. Preparation of FeP

Synthesis of β-FeOOH: In a typical procedure, 9.009 g of urea was dissolved in 200 mL of water. Then, 16.2174 g of FeCl₃·6H₂O was added to the urea solution under stirring. The pH of the solution was adjusted to 0.8 with HCl (6.0 mol L⁻¹), and the reaction system was stirred for 20 min at room temperature. The mixed solution was then heated to

boiling and refluxed under stirring in an air atmosphere for 2 h. The product was centrifuged, washed thoroughly with distilled water, and then dried at approximately 70–80 °C for 24 h.

Synthesis of FeP: 0.89 g of β-FeOOH and 4.399 g of NaH₂PO₂ were placed in two separate positions in a closed porcelain crucible with NaH₂PO₂ at the upstream side of the furnace. The molar ratio of the precursor to NaH₂PO₂ was 1:5. Subsequently, the samples were heated at 300 °C for 2 h at a heating rate of 2 °C min⁻¹ in a N₂ atmosphere. Thereafter, the crucible was cooled to ambient temperature under N₂ and the resulting FeP was collected.

2.3. Characterizations

Powder X-ray diffraction (XRD) data were acquired on a Malvern Panalytical Empyrean X-ray Diffraction diffractometer with Co K α radiation ($\lambda = 1.79 \text{ \AA}$) and operated at 35 kV and 50 mA. SEM measurements were carried out on S-4800 scanning electron microscope (SEM, Hitachi, Japan) at an accelerating voltage of 20 kV. An EDS detector coupled with SEM was used for elemental analysis. High-resolution transmission electron microscopy (HRTEM) image and selected area electron diffraction (SAED) were taken using field emission transmission electron microscopy (Tecnai G2 F30). X-ray photoelectron spectroscopy (XPS) measurements were carried out on a KRATOS XSAM800 XPS system with K α source and a charge neutralizer. The surface area of FeP sample was measured with a NOVA 4000e measuring instrument (Quantachrome Instruments) using N₂ adsorption-desorption technique at 77 K. The magnetic property measurements were performed using a physical property measurement system (PPMS-9). The DMPO trapped EPR spectrum was carried out at a MagneTech MS-5000 electron paramagnetic resonance spectroscopy (Germany). ⁵⁷Fe Mössbauer spectra were recorded on a Topologic 500A spectrometer at room temperature.

2.4. Degradation of pollutants

The working solution containing organic compounds and H₂O₂ was prepared using deionized water. The pH of this solution (pH = 3–9) was adjusted using 0.1 mol L⁻¹ HCl or 0.1 mol L⁻¹ NaOH. A total of 100 mL of the reaction solution was poured into a thermo-constant batch reactor for 5 min of preheating, after which 2 mL aliquots were obtained and filtered through a 0.22 μm nylon membrane before analysis. The reaction process was conducted under natural light, and the dosages of FeP and Fe²⁺ were 0.2 g L⁻¹ and 2.58 ppm, respectively. The temperature of the solution was maintained at 25 °C using a circulating water. The concentrations of MB in the solution before and during degradation were determined using a UV-vis spectrophotometer (UV-8000 Shanghai Metash Instruments Co. Ltd.) at 660 nm. Digital photos and UV-vis spectra obtained during the degradation process were recorded by a UV-vis optic fiber spectrometer (Ocean Optics Inc., HR 4000) via a 600 μm broadband optical fiber (Ocean Optics Inc., QP600-1-UV/vis). The corresponding synchronous screencap file was also obtained. The concentration of H₂O₂ was measured by the potassium titanium (IV) oxalate spectrophotometric method at a wavelength of 385 nm [30]. The total dissolved iron in the solution was detected using Atomic Absorption Spectrometry (VARIAN AA240FS, USA). Total organic carbon (TOC) was determined with a LiquiTOC II analyzer (Elementar Analytik, Germany).

In a typical EPR experiment, 0.02 g FeP was added to 100 mL of H₂O₂ (170–255 ppm) solution. Then, this solution was filtered through a Naflon membrane of 0.22 μm and 1 ml of supernatant was immediately injected into 1 ml of DMPO (Sigma Aldrich, 100 ppm). The obtained solution was transferred to a 100 μL capillary tube, which was then fixed in the resonant cavity of the spectrometer. To compare the catalytic activity of FeP with Fe²⁺ and iron oxide, exactly 2 mL of 129 ppm Fe²⁺ solution and 0.02 g of α-Fe₂O₃ were measured using the same procedure as references.

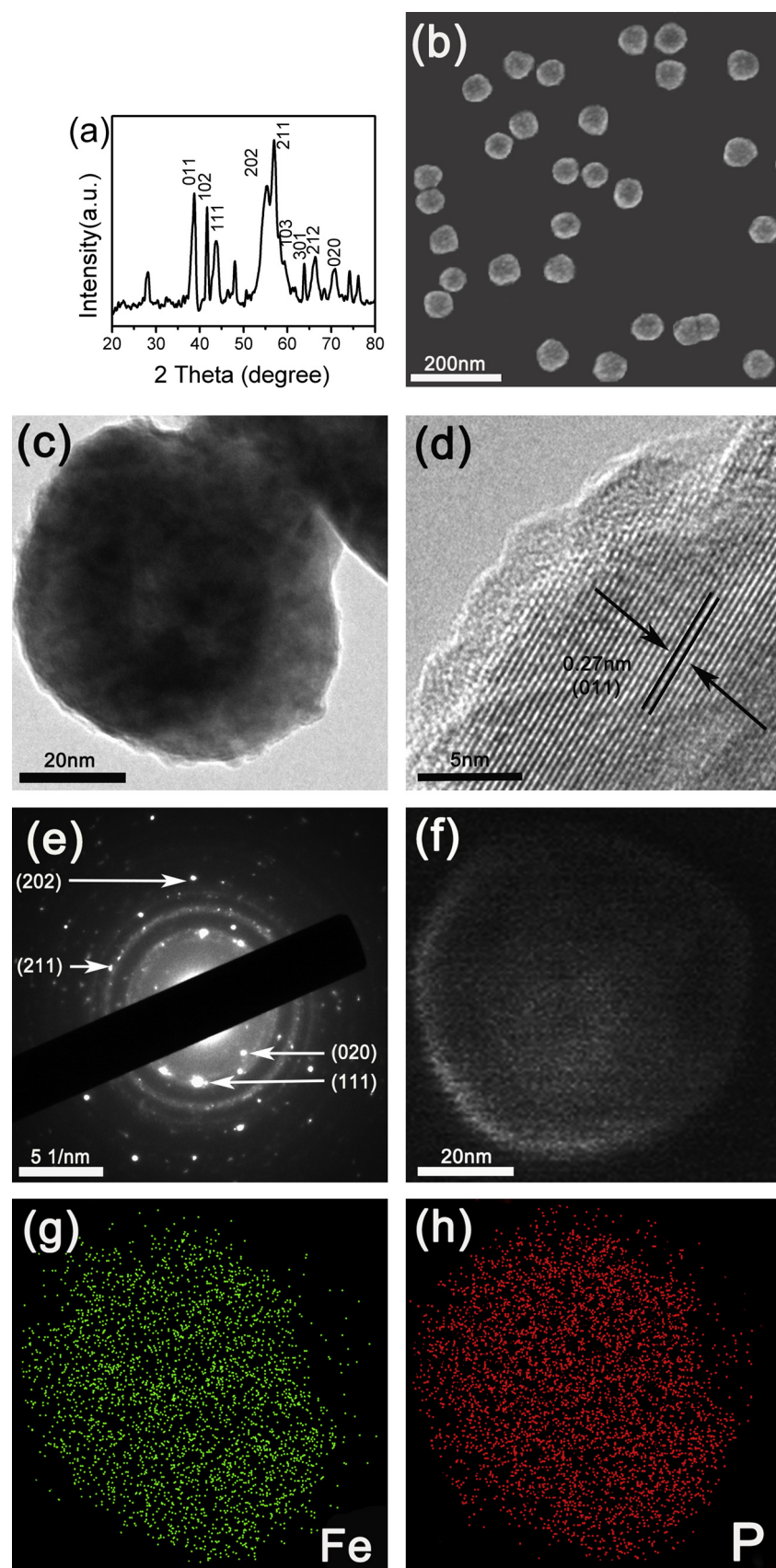


Fig. 1. XRD pattern (a), SEM image (b), TEM image (c), HRTEM image (d) and SAED pattern (e) of FeP and EDS mapping (f–h) of the marked domain in FeP.

3. Results and discussion

3.1. Characterization of FeP

XRD patterns of the phosphide product and its precursor β -FeOOH are shown in Figs. 1a and S1a, respectively. The diffraction peaks of the product can be well ascribed to the FeP phase with an orthorhombic structure (JCPDS No. 78-1443) [31], and the diffraction peaks of the precursor can be indexed to those of pure-phase β -FeOOH (JCPDS No. 00-034-1266). These findings suggest that β -FeOOH is phosphorized to form the FeP phase. The SEM image of FeP reveals that the as-prepared product is composed of a large number of uniform spheres with diameters of approximately 60–80 nm (Fig. 1b); its precursor β -FeOOH exists as rod-like particles (Fig. S1b), which further confirms the transformation from β -FeOOH to FeP. The TEM image of the as-prepared product (Fig. 1c) confirms the spherical characteristic of FeP NPs. The HRTEM image in Fig. 1d reveals a lattice fringe with an interplanar distance of 0.27 nm, which corresponds to the (011) plane of FeP. The corresponding SAED pattern of this product exhibits concentric rings composed of bright discrete diffraction spots that could be indexed to the (111), (202), (211), and (020) planes of orthorhombic FeP (Fig. 1e). The result indicates that FeP is polycrystalline in nature. Further investigation based on energy-dispersive X-ray spectroscopy (Fig. 1f-h) reveals a homogeneous distribution of Fe and P in the FeP NPs. Fig. S1c and d display the XPS spectra of FeP NPs. Two peaks at 707.0 and 711.4 eV are ascribed to Fe 2p 3/2 in FeP. The binding energy (BE) of FeP, at 707.0 eV, which is similar to that of metallic Fe (706.8 eV), is attributed to the reduced Fe species in the product. Such species are partially charged ($\text{Fe}^{\delta+}$). The peak at 711.4 eV is assigned to oxidized Fe species formed on the sample surface due to air exposure [26]. The P (2p) region reveals two peaks at 130.2 and 129.5 eV, which reflect the BEs of P 2p1/2 and P 2p3/2, respectively, and one peak at 133.7 eV [25]. The two peaks at 129.5 and 130.2 eV are attributed to metal phosphides, while the peak at 133.7 eV is assigned to oxidized P species arising from the superficial oxidation of FeP exposed to air [27]. The P 2p BE of 129.5 eV exhibits a negative shift compared with that of elemental P (130.2 eV), which suggests that P in FeP carries a partial negative charge ($\text{P}^{\delta-}$) [26]. The specific surface area of FeP calculated from its N_2 adsorption-desorption isotherm is $60.79 \text{ m}^2 \text{ g}^{-1}$ (Fig. S1e). Fig. S1f indicates that as-prepared FeP exhibits superparamagnetism [32], and its saturated magnetization is approximately 30 emu g^{-1} .

3.2. Co-catalytic performance of FeP/Fe^{II} for HO[·] production and MB degradation

The catalytic property of FeP for H_2O_2 decomposition was evaluated by EPR and compared with those of Fe^{2+} and $\alpha\text{-Fe}_2\text{O}_3$. DMPO-trapped EPR spectra generated from FeP reveal that, unlike homogeneous (Fe^{2+}) and heterogeneous Fenton systems ($\alpha\text{-Fe}_2\text{O}_3$), our catalytic

system has much higher catalytic activity for H_2O_2 decomposition and HO^{\cdot} generation under the same experiment conditions (Fig. 2a). Considering that FeP NPs are superparamagnetic, the magnetic field of an EPR spectrometer probably induces the agglomeration of FeP NPs and causes undesirable non-resonant losses of microwave energy [12]. In addition, a strong ferromagnetic resonance signal resulting from these NPs overlaps with the weak lines from spin adducts [12]. To avoid these influences, the FeP NPs were incubated with a H_2O_2 and DMPO solution and magnetically separated rapidly to obtain a clear supernatant; the latter was used for EPR measurements. Weak EPR signals were observed upon incubation of H_2O_2 and DMPO solutions with $\alpha\text{-Fe}_2\text{O}_3$ NPs (Fig. 2a). Incubation of H_2O_2 and DMPO with Fe^{2+} solution resulted in a strong four-line EPR signal with a 1:2:2:1 peak-to-peak intensity pattern. The four lines with approximately equal spacing of ca. 1.49 mT are consistent with the hyperfine splitting reported for the DMPO- HO^{\cdot} spin adduct [5,12]. The magnitude of the DMPO- HO^{\cdot} adduct EPR signal in FeP system increased by 1.8- and 10.0-fold compared with those in the homogeneous Fenton and $\alpha\text{-Fe}_2\text{O}_3$ heterogeneous Fenton systems, respectively. Actually, the degradation rate of MB in FeP system is much larger than those in Fe^{2+} and $\alpha\text{-Fe}_2\text{O}_3$ systems (Fig. S2), which further supports the above conclusion.

The special structure of FeP is considered essential for the observed much higher catalytic performance than that of traditional Fe-based compound. This is because Fe carries partial positive charges ($\text{Fe}^{\delta+}$, $0 < \delta^+ < 2$) and P carries partial negative charges ($\text{P}^{\delta-}$, $-1 < \delta^- < 0$) in FeP [25–27]. Besides $\text{Fe}^{\delta+}$, we speculated that $\text{P}^{\delta-}$ in FeP should have some activity for the production of HO^{\cdot} , since Lyu et al. [33] found that the electron-rich center around O in phenoxylphenol-functionalized reduced graphene oxide nanosheets could reduce H_2O_2 to produce HO^{\cdot} . To confirm this speculation, the EPR spectrum of red phosphorus was determined and weak EPR signals were observed. About 7.88% MB degradation was obtained (Fig. S3). Theoretically, the catalytic activity of $\text{P}^{\delta-}$ in FeP should be better than that of element phosphorus.

To investigate the effect of pH on the HO^{\cdot} production in our system, EPR spectra were tested at different pH, and the results are shown in Fig. S4. The EPR spectra were recorded at 90 s intervals for each system. Plotting the intensity of the EPR signals against the reaction times produced straight lines (Fig. 2b), the slopes of which could be used to evaluate the generation rates of HO^{\cdot} radicals [34]. The slopes provided overall HO^{\cdot} generation rates of 0.85, 0.52, 0.38, 0.25, and 0.18 s^{-1} for systems of pH 3, 4, 5, 6, and 7, respectively. FeP exhibits high catalytic activity for H_2O_2 decomposition at pH 3. However, the decomposition rate of H_2O_2 on FeP toward the generation of HO^{\cdot} decreased with increasing pH. Considering the possible contribution of leached Fe ions to the reaction at pH 3, the FeP sample was added to deionized water of pH 3 and stirred for 30 min. Then, the FeP NPs were separated, the clear supernatant was incubated with a H_2O_2 and DMPO solution, and the EPR spectrum of the solution was measured. In the absence of a solid

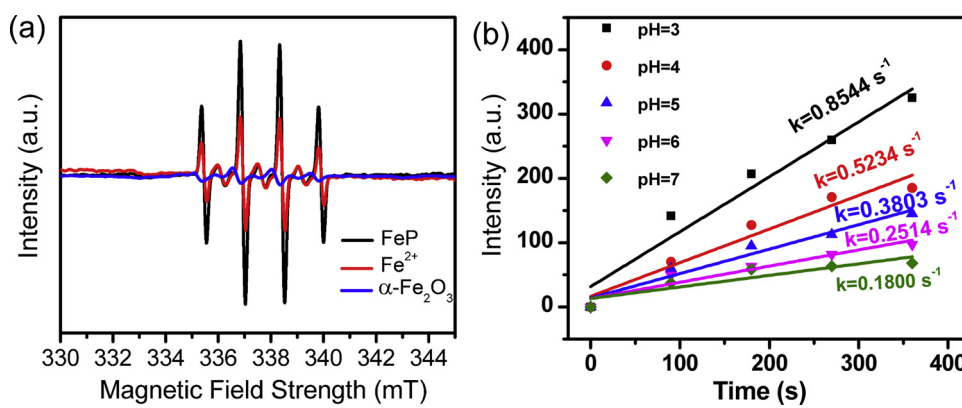


Fig. 2. (a) EPR spectra over FeP (0.2 g L^{-1}), Fe^{2+} (2.58 ppm) and $\alpha\text{-Fe}_2\text{O}_3$ (0.2 g L^{-1}), H_2O_2 : 170 ppm , pH = 3; (b) Production rate of HO^{\cdot} calculated by EPR.

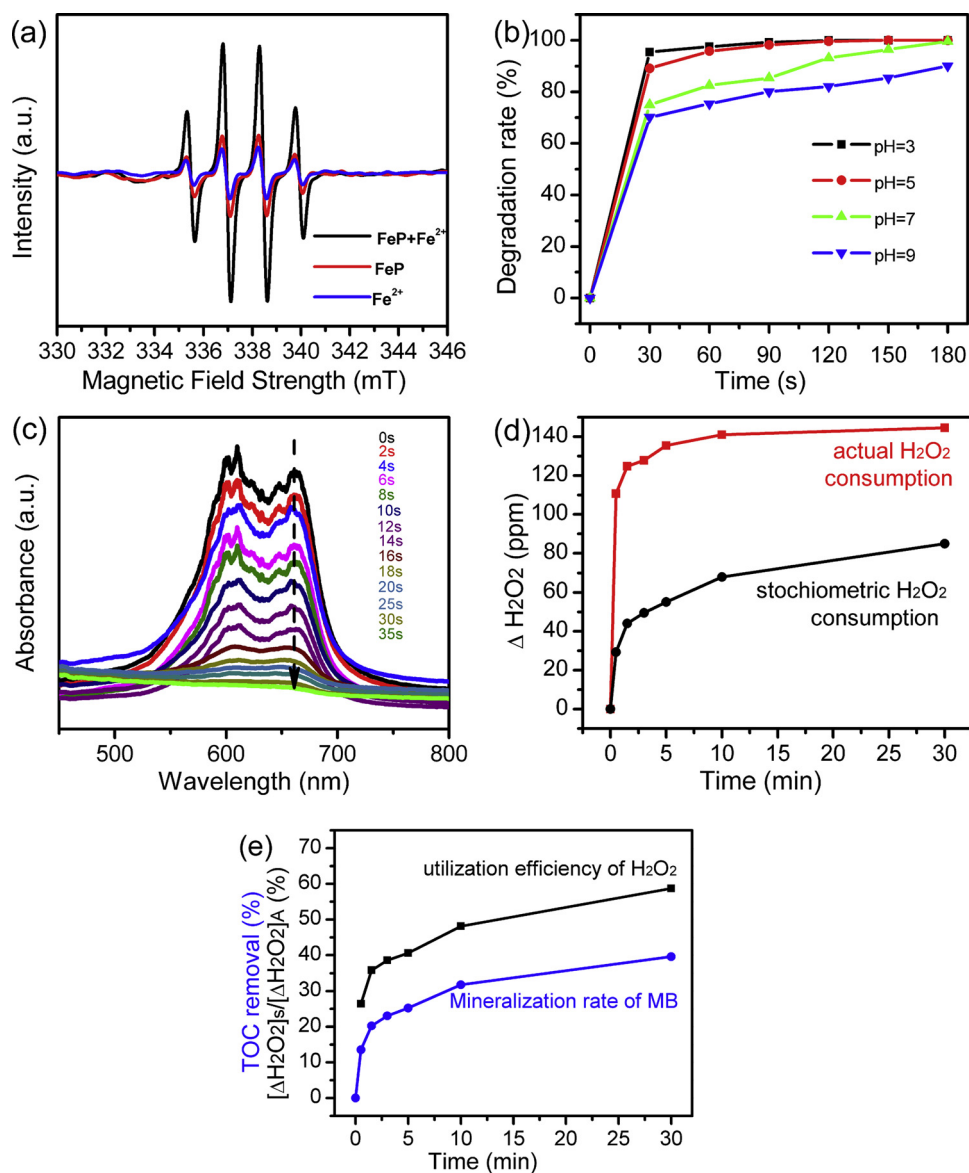


Fig. 3. (a) EPR spectra of FeP, Fe^{2+} and $\text{FeP}/\text{Fe}^{\text{II}}$ systems; (b) The changes of the degradation rate of MB with time at different pHs; (c) The absorption spectra of the reaction system for degradation MB recorded by UV-vis optic fiber spectrometer. (d) Changes of the actual and stoichiometric consumption of H_2O_2 with time. (e) The utilization efficiency of H_2O_2 and TOC removal during the reaction of 30 min. Other parameters: $\text{FeP}: 0.2 \text{ g L}^{-1}$, $\text{Fe}^{2+}: 2.58 \text{ ppm}$; $\text{H}_2\text{O}_2: 255 \text{ ppm}$, $\text{MB}: 100 \text{ ppm}$.

catalyst, the amplitude of EPR signals from DMPO spin adducts was much lower than that in presence of a solid catalyst (Fig. S4a and f), thus suggesting that the strong EPR signal at pH 3 is not mainly caused by leached Fe ions. The leached Fe ions may only play a triggering role in H_2O_2 decomposition.

To confirm that the co-existence of FeP and trace Fe^{2+} could improve HO^\cdot production, the EPR spectra of three systems with FeP only, Fe^{2+} only, and $\text{FeP}/\text{Fe}^{\text{II}}$ were determined (Fig. 3a). The starting Fe^{2+} reveals poor activity for HO^\cdot production at pH 7. However, the $\text{FeP}/\text{Fe}^{\text{II}}$ co-catalyst resulted in strong HO^\cdot signals, that is, the intensity of the co-catalyst is much larger than the sum of the signals of individual species. As such, synergistic effects must exist among these species. MB degradation was investigated as the model system for the $\text{FeP}/\text{Fe}^{\text{II}}$ co-catalyst. Rapid MB degradation was observed over a wide pH range from 3.0 to 9.0 (Fig. 3b). For example, 95.74% and 89.01% of the MB in solution was degraded within 30 s at pH 3 and pH 5, respectively. Even at pH 7, 93.11% of the MB was degraded within 2 min and 99.65% within 3 min. To clearly observe the degradation process of MB, the ultraviolet-visible (UV-vis) spectra of the system, as recorded by a

UV-vis optic fiber spectrometer at time intervals of 1 s are displayed in Fig. 3c. The corresponding synchronous screen CAP file is provided in the Supporting Information (SI) section. Approximately 53.5% of the MB in a 100 ppm solution was degraded within 10 s (Fig. 3c), while approximately 88.2% of the dye was degraded within 20 s.

Considering that the rapid degradation of MB by spectrum method may be resulted from its decoloring, the H_2O_2 decay and TOC decay with time were determined and the utilization efficiency of H_2O_2 was calculated according to previously described method (see SI) [20,35]. The results are shown in Fig. 3d and e. The actual consumption of H_2O_2 is much larger than its stoichiometric consumption in the first 30 s (Fig. 3d). The utilization efficiency of H_2O_2 is 27.1% within 30 s (Fig. 3e), indicating that the first formed HO^\cdot was mainly used to destroy the chromophore of MB and leading to a complete decolorization of MB. After 30 s, the utilization efficiency of H_2O_2 began to increase, reaching 58.71% at 30 min, and the mineralization rate of MB at this time was about 40%. The difference between them should be attributed to that part HO^\cdot was used to destroy the structure of intermediate products to form small-molecule products instead of complete

Table 1

Comparison of the degradation of MB with different catalysts.

Catalyst	Catalyst ^a (g L ⁻¹)	MB ^b (ppm)	H ₂ O ₂ ^c (mM)	Time (min)	TOC ^d (%)	c/b	d/a	d/c	Ref.
Fe-Mn binary oxide	1	100	286	120	31.4	2.86	31.4	0.11	[36]
α-Fe ₂ O ₃ @GO + UV	0.25	40	—	80	56	—	224	—	[37]
Si-Al/α-FeOOH	1	20	200	60	72	10	72	0.36	[38]
Fe ₃ O ₄ reduced with H ₂	3	100	300	120	75	3	25	0.25	[39]
MPCMSS + NH ₂ OH	2	40	16	—	68	0.4	34	4.25	[40]
FeP/ Fe ^{II}	0.2	100	7.5	30	45	0.075	225	6	This study
FeP/ Fe ^{II}	0.2	100	13.65	30	60	0.137	300	4.4	This study

Note: c/b: H₂O₂ consumption per ppm MB degradation.

d/a: TOC decay per gram catalyst.

d/c: TOC decay per mmol H₂O₂ consumption.

oxidation to CO₂ and water [36]. Table 1 presents a comparison of the catalytic performance between the current system and other studies [36–40]. The mineralization rate of MB in the current system was not the best because of its low catalyst and H₂O₂ dosage and a high MB concentration. However, all of these factors could influence TOC removal efficiency because a high TOC removal could be achieved by prolonging reaction time or constantly maintaining high level H₂O₂ after breaking down the chromophore group of dye molecule [37,38,41]. When the results were normalized to the same scale, the current system exhibited an obvious advantage (Table 1). In fact, when H₂O₂ dosage was increased to 464 ppm, the utilization efficiency of H₂O₂ reached 66.4% at 30 min, and the mineralization rate of MB was increased from 40% to 57.6% at 30 min. These results mean that high H₂O₂ dosage, for a certain concentration of pollutant, is necessary to realize a high mineralization ratio.

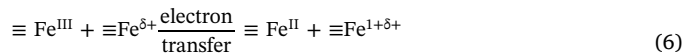
In addition, test on Fe leaching from FeP catalyst was conducted at pH 3 and the result indicated that 0.51 ppm of total iron ions was detected within 30 min (Fig. S5a). For the co-catalyst system of FeP/Fe^{II} and H₂O₂, the residual content of Fe ions in the solution (2.67 ppm) was slightly larger than 2 ppm only at pH 3 and the residual contents of Fe ions at pH 5–9 were below the limitation of Fe in EU and US standards (< 2 ppm) [5] (Fig. S5b). The activity of FeP after seven cycles of reaction is nearly the same as that of the freshly prepared catalyst (Fig. S5c). All of these results indicated that FeP has excellent stability and reusability. Additionally, the superparamagnetism of FeP is favorable for its separation from the reaction system (Fig. S1f).

To understand the degradation pathway of MB, ESI-MS analysis was employed to investigate the degradation products of MB (Fig. S6). Because MB degradation occurred rapidly, the MB concentration of the test solution was increased to 500 ppm to obtain information about the degradation products. Analysis of pure MB by ESI-MS indicated a major peak at *m/z* 284 corresponding to the molecular ion peak of MB (Fig. S6a) [42]. No peaks were observed at low or high *m/z* values, thereby indicating that the ESI-MS technique does not cause any further MB degradation or polymerization. After degradation, the peak at *m/z* 284 disappeared, which suggests that the MB molecules are completely consumed. During a reaction process, 10 new species with *m/z* 272, 220, 195, 179, 163, 148, 120, 117, 110, and 102 were detected; these species were attributed to C₁₄H₁₄N₃SO, C₇H₁₀NSO₅, C₄H₅NSO₆, C₄H₅NSO₅, C₄H₅NSO₄, C₄H₄O₆, C₄H₈O₄, C₄H₅O₄, C₆H₈NO, and C₄H₆O₃, respectively (Fig. S6b). After the degradation reaction, five peaks at *m/z* 179, 163, 120, 117, and 102 were observed (Fig. S6c). However, compared with Fig. S6b, the intensities of the peaks at 120, 117, and 102 increased whereas those of 179 and 163 peaks decreased, which suggests that only 120, 117, and 102 peaks are the final products. Therefore, a possible MB degradation mechanism is proposed in the current system (Fig. 4).

3.3. Co-catalytic mechanism of FeP/Fe^{II} for the efficiency production of HO[·]

Previous studies demonstrate that when Fe²⁺ is adsorbed by an Fe oxide or Fe mineral surface, it displays enhanced reductive abilities toward environmental contaminants compared with aqueous Fe²⁺ alone [43–46]. This effect is not limited to Fe^{III} (oxyhydr)oxides, as similar rate enhancements have been observed when Fe^{II} is adsorbed onto kaolinite [47] and nontronites [48]. Studies indicate that Fe²⁺ rarely exists as stable adsorbed species on Fe oxides. Fe²⁺ is usually oxidized to a bound ≡Fe^{III} atom through electron transfer between Fe²⁺ and structural ≡Fe^{III} in the Fe oxide lattice [43]. Electrons could also be transferred from Fe⁰ to Fe^{III} in Fe₃O₄ [39]. This type of internal electron conduction affects interfacial reaction rates [29].

The results in the current system and previous references suggest that the catalytic mechanism of FeP is mainly attributed to three paths (Scheme 1). **Path 1:** Fe in FeP carries partial δ⁺ charges, and ≡Fe^{δ+} can function as an active site for H₂O₂ decomposition (Figs. 2 and S3b). **Path 2:** P in FeP carries partial negative charges (P^{δ-}, -1 < δ < 0). The electron-rich center around P may function as an active site to reduce H₂O₂ and produce HO[·]. The results in Fig. S3 support this conclusion. Additionally, EPR spectrum at neutral pH (Fig. S4) should be attributed to the contribution of both Fe and P in FeP instead of leached Fe ions. **Path 3:** The added Fe²⁺ is first adsorbed on the FeP surface and becomes ≡Fe^{II}. Compared with dissolved Fe²⁺, ≡Fe^{II} has a more negative reduction potential [43–46], which results in its strong catalytic activity for H₂O₂ decomposition. Hereafter, a cycle of ≡Fe^{II} ↔ ≡Fe^{III} occurring on the FeP surface is established. Similar to other heterogeneous Fenton systems, the reaction from ≡Fe^{III} to ≡Fe^{II} (Eq. 4) is the rate-limiting step of the whole cycle. However, apart from Eq. 4, another path can be used (Eq. 6) to recover ≡Fe^{II} in the current system. That is, the structural Fe^{δ+} atom in FeP can donate an electron to ≡Fe^{III}, giving rise to ≡Fe^{II}. Fe^{δ+} transforms into ≡Fe^{1+δ+}, which returns to Fe^{δ+} by extracting an electron from the bulk of FeP. Thus, a cycle of Fe^{δ+} → ≡Fe^{1+δ+} → Fe^{δ+} is simultaneously established.



Some considerations support this electron transfer: (i) Metallic FeP presents high electrical conductivity, which is important for electron transport [49,50]. (ii) P networks in FeP are similar to those of graphene [28] and allow electrons to move through this network. A uniform distribution of Fe and P in the FeP is favorable for the electron transfer within FeP (Fig. 1g and h). (iii) The negative shift of the P 2p XPS spectrum (Fig. S1d) suggests improved electron-donating ability [51]. Moreover, the recovery rate of ≡Fe^{II} by Eq. 6 is expected to become a rapid process because the observation of a fully averaged state at 110 K indicates that the activation energy of electron transfer is less than 0.1 eV [52]. Once the two cycles ((1) ≡Fe^{III} → ≡Fe^{II} → ≡Fe^{III} and (2) Fe^{δ+} → ≡Fe^{1+δ+} → Fe^{δ+}) are established on the FeP interface, a steady supply of surface ≡Fe^{II} could rapidly decompose H₂O₂ to

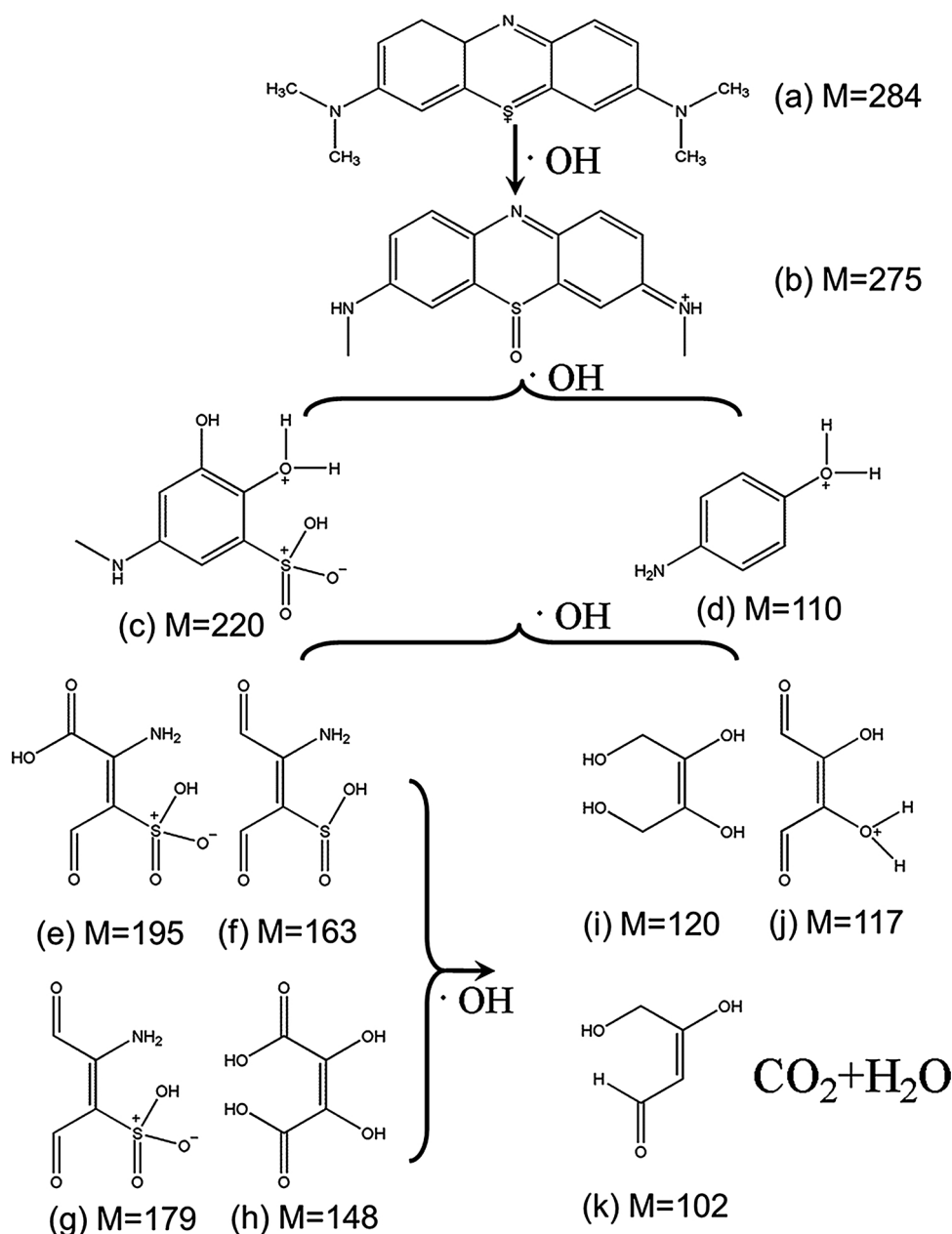


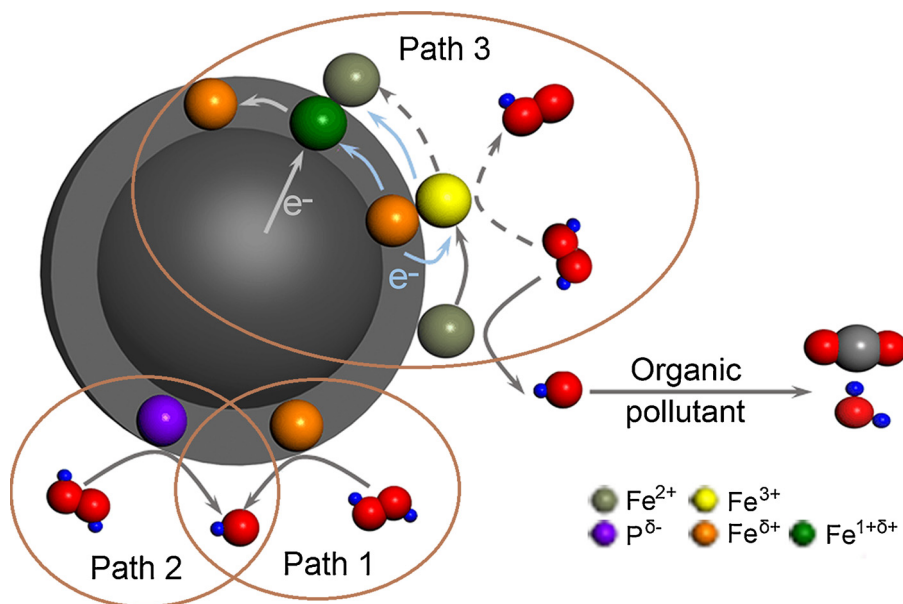
Fig. 4. Proposed degradation pathway of MB by FeP/Fe^{II} Fenton process.

generate abundant HO[·] and degrade pollutants.

To confirm this mechanism of Path 3, a series of experiments were performed. First, the sample after degradation was characterized by XPS (Fig. S7). No perceptible changes were observed in the XPS spectra of the sample FeP before and after one cycle of degradation reaction. Considering that Mössbauer spectroscopy (MS) is a powerful probe to identify Fe local structure and its parameters are sensitive to any variation in the chemical environment of Fe atom, the second experiment was conducted to characterize the FeP samples before and after degradation by MS. In this experiment, the selected FeP samples were subjected to 20 cycles of degradation at pH 3 and 7. The MS results at room temperature are indicated in Fig. 5. The fitting parameters of isomer shift (IS), quadrupole splitting (QS), half peak width, and absorption area proportion are summarized in Table 2.

Fig. 5 illustrates the MS consists of three different components: two doublet peaks and one sextuplet. The IS parameter is mainly related to the oxidation state of the Fe ion, and QS describes the symmetry of the charge distribution around the Fe nucleus [53]. In the FeP sample

before degradation, one doublet had an IS of 0.31 mm/s and a QS of -0.27 mm/s, which could be ascribed to the FeP phase, accounting for 60.08% of iron species [32,54]. The second doublet had an IS of 1.05 mm/s and a QS of 2.67 mm/s, which was closed to Fe^{II} phases (called Fe^{II}-like), representing 11.18% of the iron species in the system [55,56]. The sextuplet with an IS of 0.37 mm/s and a QS of -0.27 mm/s could be ascribed to the Fe^{III} phase, which accounts for 28.74% of iron species [57]. Fe^{III} phase was assigned to the oxidized Fe species, consistent with the XPS results (Fig. S1c). The Fe^{II}-like species, probably located at the junction of Fe^{δ+} and Fe^{III}, was resulted from the electron transfer from Fe^{δ+} to Fe^{III}. Although the three sub-spectra were also detected in the FeP sample after 20 cycles of degradation, the proportion of the three different components changed. After degradation, the proportions of FeP decreased from 60.08% to 56.88% and 56.18% at pH 3 and 7, respectively, whereas the proportions of Fe^{II}-like phase increased from 11.18% to 16.30% and 18.61%. Therefore, electron transfers in FeP occurred during the reaction. In addition, the proportion of Fe^{III} after reaction decreased from 28.74% to 26.82% (at pH 3)



Scheme 1. Schematic illustration for the possible hydroxyl radical generation mechanism for the FeP/Fe^{II} Fenton-like catalyst.

and 25.21% (at pH 7), which could be attributed to the electron transfer from FeP to Fe^{III} phase, thus transforming a part of Fe^{III} into Fe^{II}. These results confirm the existence of the process described in Eq. 6. Further evidence of the electron transfer was confirmed by density functional theory (DFT) calculations (see SI) (Fig. 5d). The results indicated that the Bader charge of Fe on the surface of FeP before reaction was +0.41|e|, whereas that after H₂O₂ decomposition was +0.49|e|, consistent with the MS findings.

The third experiment was conducted to confirm the electron transfer process in the current system by adding Fe³⁺ instead of Fe²⁺ to the reaction system. The EPR spectrum and the degradation rate of MB at different pH were detected, and the findings are shown in Fig. 6a and b. Similar to the system triggered by Fe²⁺ (Fig. 3), the starting Fe³⁺

indicated activity for HO[·] production at pH 7, whereas the coexistence of FeP/Fe^{III} resulted in strong HO[·] signals (Fig. 6a). Rapid MB degradation was also observed over a wide pH range of 3.0–9.0 (Fig. 6b), and the contribution of alone Fe³⁺ on the MB degradation could be ignored (Fig. S8a). Comparing Figs. 3b and 6b, the degradation times at the same pH were nearly equal. When Fe³⁺ was introduced to the FeP system, the ions were initially adsorbed on the FeP surface to become ≡Fe^{III} and then gained electrons from structural Fe^{δ+} through electron transfer, resulting in the formation of ≡Fe^{II}. Subsequent reactions are identical to those previously described. The residual content of Fe in the solution after reaction was below the limitation of Fe in EU and US standards (< 2 ppm) (Fig. S8b).

The fourth experiment was performed to compare the degradation

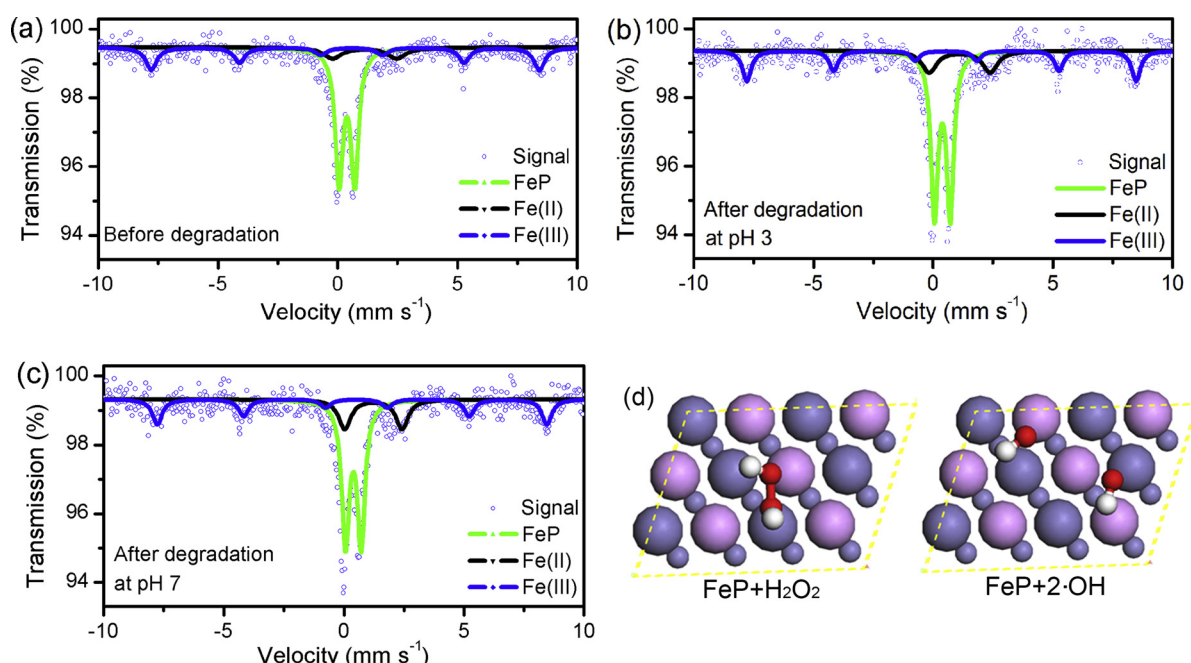


Fig. 5. Mossbauer spectra of the FeP samples. (a) before degradation; (b) after degradation of 20 cycles at pH 3; (c) after degradation of 20 cycles at pH 7; (d) The optimized structure for the reaction of decomposition of H₂O₂ in FeP/H₂O₂ system and FeP/2HO[·] system. Atom coloring: Fe (purple), P (pink), O (red) and H (white) (For interpretation of the references to colour in this figure legend, the reader is referred to the web version of this article).

Table 2

Mössbauer hyperfine parameters derived from Mössbauer spectra.

Sample		IS (mm/s)	QS (mm/s)	Line Width (mm/s)	Spectral Area (%)	Assignment
Before degradation	Doublet	0.31	0.65	0.37	60.08	FeP
	Doublet	1.05	2.67	0.87	11.18	Fe(II)-like
	Sextuplet	0.37	-0.27	0.54	28.74	Fe(III)
After degradation at pH 3	Doublet	0.31	0.66	0.35	56.88	FeP
	Doublet	1.04	2.54	0.76	16.3	Fe(II)-like
	Sextuplet	0.37	-0.21	0.44	26.82	Fe(III)
After degradation at pH 7	Doublet	0.32	0.65	0.38	56.18	FeP
	Doublet	1.15	2.39	0.61	18.61	Fe(II)-like
	Sextuplet	0.36	-0.18	0.48	25.21	Fe(III)

rate of MB in FeP/Fe^{II} system with that in α -Fe₂O₃/Fe^{II} system. The degradation process of MB was investigated at pH 7, and the results are displayed in Fig. 6c. Without Fe²⁺ addition, the degradation rates of MB at 1 min in FeP and α -Fe₂O₃ systems were very low at pH 7. When trace Fe²⁺ was introduced to the FeP and α -Fe₂O₃ systems, the degradation rate of MB prominently increased and reached nearly 100% at 40 s, whereas that in the α -Fe₂O₃ system was only 30% at 1 min. The increment of MB degradation rate in the FeP system ($\Delta 2$) was larger than that in the α -Fe₂O₃ system ($\Delta 1$). For convenience, the rate coefficients of Eqs. 4 and 5 were assumed to be identical for the two systems. Thus, $\Delta 3$ in Fig. 6c could be attributed to the contribution of Eq. 6 in the FeP system because the path of Eq. 6 does not exist in the α -Fe₂O₃ system.

Overall, the co-catalyst of FeP/Fe^{II} greatly enhanced the decomposition of H₂O₂ and production of HO[·]. Among them, trace Fe²⁺ adsorbed on FeP NPs triggered surface Fenton reaction and then was oxidized to \equiv Fe^{III}. The unique structure of FeP makes it could donate electrons to those new formed \equiv Fe^{III}, which accelerates the cycle from \equiv Fe^{III} to \equiv Fe^{II} (the rate-limiting step) in heterogeneous Fenton reaction. Both Fe and P in FeP could act as active sites for the decomposition of H₂O₂, but have to work with the trace Fe²⁺ to achieve high

performance.

4. Conclusions

In summary, we demonstrated that the coexistence of FeP and trace Fe²⁺ can greatly improve the reduction of Fe^{III} to Fe^{II} over a wide pH range (pH = 3–9), resulting in rapid H₂O₂ decomposition and MB degradation (ca. ~30 s under optimum conditions). H₂O₂ decomposition in the current system can be completed via three paths. (1) Fe in FeP carries partial δ^+ charges and functions as an active site for H₂O₂ decomposition and HO[·] production. (2) P in FeP carries partial δ^- charges and also functions as an active site for H₂O₂ decomposition. (3) More importantly, the coexistence of FeP and trace Fe²⁺ results in the production of \equiv Fe^{II} on the surface of FeP, and a surface Fenton system is rapidly established on FeP. Electron transfer from structural Fe⁸⁺ to \equiv Fe^{III} accelerates the conversion from \equiv Fe^{III} to \equiv Fe^{II} and the reaction rate of pollutant degradation. The catalytic properties of FeP are particularly interesting not only for its high catalytic efficiency and stability during catalytic cycle but also for the mechanism to accelerate the cycle of \equiv Fe^{III} \leftrightarrow \equiv Fe^{II}. This study provides a new Fenton-like oxidation system for pollutant control and introduces an exciting field of

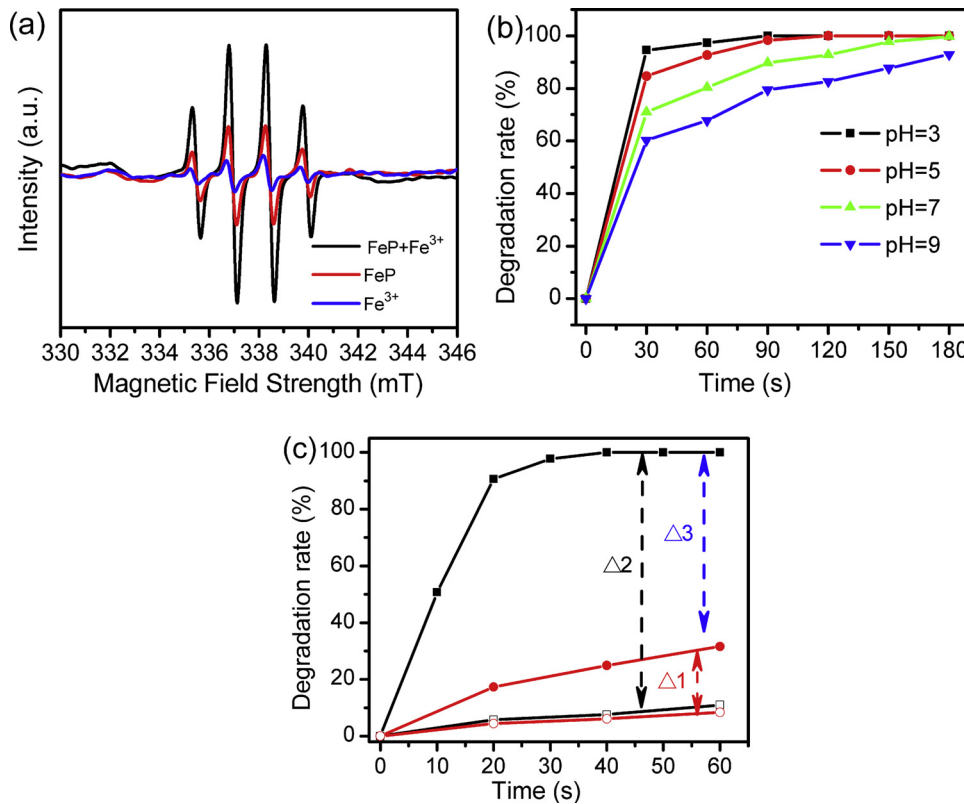


Fig. 6. (a) EPR spectra of FeP, Fe³⁺ and FeP/Fe³⁺ systems; (b) The changes of the degradation rate of MB with time in FeP/Fe^{III} system; (c) Comparison of catalytic activity of FeP/Fe^{II} and α -Fe₂O₃/Fe^{II} at pH 7. ■: FeP/Fe^{II}, □: FeP, ●: α -Fe₂O₃/Fe^{II} and ○: α -Fe₂O₃. Other parameters: FeP: 0.2 g L⁻¹, Fe³⁺: 5.15 ppm; Fe²⁺: 2.58 ppm; H₂O₂: 255 ppm, MB: 100 ppm.

study. As an ecofriendly magnetic material, FeP exhibits excellent co-catalytic performance for HO[·] production by decomposing H₂O₂, thereby highlighting the practical utility of FeP for environmental applications.

Declaration of Competing Interest

The authors declare that they have no known competing financial interests or personal relationships that could have appeared to influence the work reported in this paper.

Acknowledgments

Can Ma and Shuo Feng contributed equally. The authors are grateful to the National Natural Science Foundation of China (No. 21277040 and 21477032), Natural Science Foundation of Hebei Province (No. B2017205166) and Technology Innovation Project of Hebei Normal University (No. L2018K06).

Appendix A. Supplementary data

Supplementary material related to this article can be found, in the online version, at doi:<https://doi.org/10.1016/j.apcatb.2019.118015>.

References

- [1] X.N. Li, X. Huang, S.B. Xi, S. Miao, J. Ding, W.Z. Cai, S. Liu, X.L. Yang, H.B. Yang, J.J. Gao, J.H. Wang, Y.Q. Huang, T. Zhang, B. Liu, Single cobalt atoms anchored on porous N-doped graphene with dual reaction sites for efficient Fenton-like catalysis, *J. Am. Chem. Soc.* 140 (2018) 12469–12475.
- [2] C.C. Dong, J.H. Ji, B. Shen, M.Y. Xing, J.L. Zhang, Enhancement of H₂O₂ decomposition by the co-catalytic effect of WS₂ on the Fenton reaction for the synchronous reduction of Cr(VI) and remediation of phenol, *Environ. Sci. Technol.* 52 (2018) 11297–11308.
- [3] A.L.T. Pham, F.M. Doyle, D.L. Sedlak, Kinetics and efficiency of H₂O₂ activation by iron-containing minerals and aquifer materials, *Water Res.* 46 (2012) 6454–6462.
- [4] Y. Qin, F. Song, Z. Ai, P. Zhang, L. Zhang, Protocatechuic acid promotedalachlor degradation in Fe(III)/H₂O₂ Fenton system, *Environ. Sci. Technol.* 49 (2015) 7948–7956.
- [5] X.J. Yang, X.M. Xu, J. Xu, Y.F. Han, Iron oxychloride (FeOCl): an efficient Fenton-like catalyst for producing hydroxyl radicals in degradation of organic contaminants, *J. Am. Chem. Soc.* 135 (2013) 16058–16061.
- [6] W.H. Ma, J. Li, X. Tao, J. He, Y.M. Xu, J.C. Yu, J.C. Zhao, Efficient degradation of organic pollutants by using dioxygen activated by resin-exchanged iron(II) bipyridine under visible irradiation, *Angew. Chem. Int. Ed.* 42 (2003) 1029–1032.
- [7] L. Chen, J. Ma, X. Li, J. Zhang, J. Fang, Y. Guan, P. Xie, Strong enhancement on Fenton oxidation by addition of hydroxylamine to accelerate the ferric and ferrous iron cycles, *Environ. Sci. Technol.* 45 (2011) 3925–3930.
- [8] L. Xu, J. Wang, A heterogeneous Fenton-like system with nanoparticulate zero-valent iron for removal of 4-chloro-3-methyl phenol, *J. Hazard. Mater.* 186 (2011) 256–264.
- [9] G.K. Zhang, Y.Y. Gao, Y.L. Zhang, Y.D. Guo, Fe₂O₃-pillared rectorite as an efficient and stable Fenton-like heterogeneous catalyst for photodegradation of organic contaminants, *Environ. Sci. Technol.* 44 (2010) 6384–6389.
- [10] Z.C. Ma, L.M. Ren, S.T. Xing, Y.S. Wu, Y.Z. Gao, Sodium dodecyl sulfate modified FeCo₂O₄ with enhanced Fenton-like activity at neutral pH, *J. Phys. Chem. C* 119 (2015) 23068–23074.
- [11] A.D. Bokare, W. Choi, Review of iron-free Fenton-like systems for activating H₂O₂ in advanced oxidation processes, *J. Hazard. Mater.* 275 (2014) 121–135.
- [12] M.A. Voinov, J.O.S. Pagán, E. Morrison, T.I. Smirnova, A.I. Smirnov, Surface-mediated production of hydroxyl radicals as a mechanism of iron oxide nanoparticle biotoxicity, *J. Am. Chem. Soc.* 133 (2011) 35–41.
- [13] M. Sun, C.H. Chu, F.L. Geng, X.L. Lu, J.H. Qu, J. Crittenden, M. Elimelech, J.-H. Kim, Reinventing Fenton chemistry: iron oxychloride nanosheet for pH insensitive H₂O₂ activation, *Environ. Sci. Technol. Lett.* 5 (2018) 186–191.
- [14] J. Zhang, X.L. Jiao, Y.G. Xia, F.F. Liu, Y.P. Pang, X.F. Zhao, D.R. Chen, Enhanced catalytic activity in liquid-exfoliated FeOCl nanosheets as a Fenton-like catalyst, *Chem. Eur. J.* 22 (2016) 9321–9329.
- [15] J. Zhang, M.Y. Zhan, L.L. Zheng, C. Zhang, G.D. Liu, J.Q. Sha, S.J. Liu, S. Tian, FeOCl/POM heterojunctions with excellent Fenton catalytic performance via different mechanisms, *Inorg. Chem.* 58 (2019) 250–258.
- [16] J. Zhang, M.X. Yang, Y. Lian, M.L. Zhong, J.Q. Sha, G.D. Liu, X.F. Zhao, S.J. Liu, Ce³⁺ self-doped CeO_x/FeOCl: an efficient Fenton catalyst for phenol degradation under mild conditions, *Dalton Trans.* 48 (2019) 3476–3485.
- [17] J. Zhang, G.D. Liu, P.H. Wang, S.J. Liu, Facile synthesis of FeOCl/iron hydroxide hybrid nanosheets: enhanced catalytic activity as a Fenton-like catalyst, *New J. Chem.* 41 (2017) 10339–10346.
- [18] G.M.S. Elshafei, A.M. Al-Sabagh, F.Z. Yehia, C.A. Philip, N.A. Moussa, Gh. Eshaq, A.E. ElMetwally, Metal oxychlorides as robust heterogeneous Fenton catalysts for the sonophotocatalytic degradation of 2-nitrophenol, *Appl. Catal. B Environ.* 224 (2018) 681–691.
- [19] J. Deng, J. Jiang, Y. Zhang, X. Lin, C. Du, Y. Xiong, FeVO₄ as a highly active heterogeneous Fenton-like catalyst towards the degradation of Orange II, *Appl. Catal. B Environ.* 84 (2008) 468–473.
- [20] X.Y. Zhang, Y.B. Ding, H.Q. Tang, X.Y. Han, L.H. Zhu, N. Wang, Degradation of bisphenol A by hydrogen peroxide activated with CuFeO₂ microparticles as a heterogeneous Fenton-like catalyst: Efficiency, stability and mechanism, *Chem. Eng. J.* 236 (2014) 251–262.
- [21] J. Shi, Z. Ai, L. Zhang, Fe@Fe₂O₃ core-shell nanowires enhanced Fenton oxidation by accelerating the Fe(III)/Fe(II) cycles, *Water Res.* 59 (2014) 145–153.
- [22] J.H. Ma, W.H. Ma, C.C. Chen, H.W. Ji, J.C. Zhao, An efficient anthraquinone-resin hybrid co-catalyst for Fenton-like reactions: acceleration of the iron cycle using a quinone cycle under visible-light irradiation, *Chem. Asian J.* 6 (2011) 2264–2268.
- [23] J. Liu, C.C. Dong, Y.X. Deng, J.H. Ji, S.Y. Bao, C.R. Chen, B. Shen, J.L. Zhang, M.Y. Xing, Molybdenum sulfide co-catalytic Fenton reaction for rapid and efficient inactivation of Escherichia coli, *Water Res.* 145 (2018) 312–320.
- [24] Y.P. Zhu, C. Zeng, R.L. Zhu, Y. Xu, X.Y. Wang, H.J. Zhou, J.X. Zhu, H.P. He, TiO₂/Schwertmannite nanocomposites as superior co-catalysts in heterogeneous photo-Fenton process, *J. Environ. Sci.* 80 (2019) 208–217.
- [25] P. Jiang, Q. Liu, Y.H. Liang, J.Q. Tian, A.M. Asiri, X.P. Sun, A cost-effective 3D hydrogen evolution cathode with high catalytic activity: FeP nanowire array as the active phase, *Angew. Chem. Int. Ed.* 53 (2014) 12855–12859.
- [26] C. Lv, Z. Peng, Y. Zhao, Z. Huang, C. Zhang, The hierarchical nanowires array of iron phosphide integrated on a carbon fiber paper as an effective electrocatalyst for hydrogen generation, *J. Mater. Chem. A* 4 (2016) 1454–1460.
- [27] P. Wang, Z. Pu, Y. Li, L. Wu, Z. Tu, M. Jiang, Z. Kou, I.S. Amiuu, S. Mu, Iron-doped nickel phosphide nanosheet arrays: an efficient bifunctional electrocatalyst for water splitting, *ACS Appl. Mater. Interfaces* 9 (2017) 26001–26007.
- [28] J.H. Chen, K.H. Whitmire, A structural survey of the binary transition metal phosphides and arsenides of the d-block elements, *Coord. Chem. Rev.* 355 (2018) 271–327.
- [29] J.E. Katz, X. Zhang, K. Attenkofer, K.W. Chapman, C. Frandsen, P. Zarzycki, K.M. Rosso, R.W. Falcone, G.A. Waychunas, B. Gilbert, Electron small polarons and their mobility in iron (oxyhydr)oxide nanoparticles, *Science* 337 (2012) 1200–1203.
- [30] R.M. Sellers, Spectrophotometric determination of hydrogen peroxide using potassium titanium(IV) oxalate, *Analyst* 105 (1980) 950–954.
- [31] C. Qian, F. Kim, L. Ma, F. Tsui, P. Yang, J. Liu, Solution-phase synthesis of single-crystalline iron phosphide nanorods/nanowires, *J. Am. Chem. Soc.* 126 (2004) 1195–1198.
- [32] S. Boyanov, M. Womes, L. Monconduit, D. Zitoun, Mössbauer spectroscopy and magnetic measurements as complementary techniques for the phase analysis of FeP electrodes cycling in Li-ion batteries, *Chem. Mater.* 21 (2009) 3684–3692.
- [33] L. Lyu, G. Yu, L. Zhang, C. Hu, Y. Sun, 4-phenoxyphenol-functionalized reduced graphene oxide nanosheets: a metal-free Fenton catalyst for pollutant destruction, *Environ. Sci. Technol.* 52 (2018) 747–756.
- [34] H. Li, J. Shang, Z. Yang, W. Shen, Z. Ai, L. Zhang, Oxygen vacancy associated surface Fenton chemistry: surface structure dependent hydroxyl radicals generation and substrate dependent reactivity, *Environ. Sci. Technol.* 51 (2017) 5685–5694.
- [35] W. Luo, L. Zhu, N. Wang, H. Tang, M. Cao, Y. She, Efficient removal of organic pollutants with magnetic nanoscaled BiFeO₃ as a reusable heterogeneous Fenton-like catalyst, *Environ. Sci. Technol.* 44 (2010) 1786–1791.
- [36] J.B. Pang, F.L. Fu, W.B. Li, L.J. Zhu, B. Tang, Fe-Mn binary oxide decorated diatomite for rapid decolorization of methylene blue with H₂O₂, *Appl. Surf. Sci.* 478 (2019) 54–61.
- [37] Y.Y. Liu, W. Jin, Y.P. Zhao, G.S. Zhang, W. Zhang, Enhanced catalytic degradation of methylene blue by α-Fe₂O₃/graphene oxide via heterogeneous photo-Fenton reactions, *Appl. Catal. B Environ.* 206 (2017) 642–652.
- [38] B.L. Yuan, J.G. Xu, X.T. Li, M.L. Fu, Preparation of Si-Al/α-FeOOH catalyst from an iron-containing waste and surface-catalytic oxidation of methylene blue at neutral pH value in the presence of H₂O₂, *Chem. Eng. J.* 226 (2013) 181–188.
- [39] R.C.C. Costa, F.C.C. Moura, J.D. Ardisson, J.D. Fabris, R.M. Lago, Highly active heterogeneous Fenton-like systems based on Fe⁰/Fe₃O₄ composites prepared by controlled reduction of iron oxides, *Appl. Catal. B Environ.* 83 (2008) 131–139.
- [40] L.C. Zhou, Y.M. Shao, J.R. Liu, Z.F. Ye, H. Zhang, J.J. Ma, Y. Jia, W.J. Gao, Y.F. Li, Preparation and characterization of magnetic porous carbon microspheres for removal of methylene blue by a heterogeneous Fenton reaction, *ACS Appl. Mater. Interfaces* 6 (2014) 7275–7285.
- [41] J. He, W.H. Ma, J.J. He, J.C. Zhao, J.C. Yu, Photooxidation of azo dye in aqueous dispersions of H₂O₂/α-FeOOH, *Appl. Catal. B Environ.* 39 (2002) 211–220.
- [42] M. Roy, M.K. Naskar, Alkali metal ion induced cube shaped mesoporous hematite particles for improved magnetic properties and efficient degradation of water pollutants, *Phys. Chem. Chem. Phys.* 18 (2016) 20528–20541.
- [43] S.M. Stewart, T.B. Hofstetter, P. Joshi, C.A. Gorski, Linking thermodynamics to pollutant reduction kinetics by Fe²⁺ bound to iron oxides, *Environ. Sci. Technol.* 52 (2018) 5600–5609.
- [44] D.D. Boland, R.N. Collins, C.J. Glover, T.E. Payne, T.D. Waite, Reduction of U(VI) by Fe(II) during the Fe(II)-accelerated transformation of ferrihydrite, *Environ. Sci. Technol.* 48 (2014) 9086–9093.
- [45] A.M. Jones, A.S. Kinsela, R.N. Collins, T.D. Waite, The reduction of 4-chloronitrobenzene by Fe(II)-Fe(III) oxide systems – correlations with reduction potential and inhibition by silicate, *J. Hazard. Mater.* 320 (2016) 143–149.
- [46] E. Sylvester, L. Charlet, C. Tournassat, A. Géhin, J.-M. Grenèche, E. Liger, Redox potential measurements and Mössbauer spectrometry of Fe^{II} adsorbed onto Fe^{III}

- (oxyhydr)oxides, *Geochim. Cosmochim. Acta* 69 (2005) 4801–4815.
- [47] J. Klausen, S.P. Tröber, S.B. Haderlein, R.P. Schwarzenbach, Reduction of substituted nitrobenzenes by Fe(II) in aqueous mineral suspensions, *Environ. Sci. Technol.* 29 (1995) 2396–2404.
- [48] T.B. Hofstetter, R.P. Schwarzenbach, S.B. Haderlein, Reactivity of Fe(II) species associated with clay minerals, *Environ. Sci. Technol.* 37 (2003) 519–528.
- [49] J. Ryu, N. Jung, J.H. Jang, H.-J. Kim, S.J. Yoo, In situ transformation of hydrogen-evolving CoP nanoparticles: toward efficient oxygen evolution catalysts bearing dispersed morphologies with Co-oxo/hydroxo molecular units, *ACS Catal.* 5 (2015) 4066–4074.
- [50] Y.-P. Zhu, Y.-P. Liu, T.-Z. Ren, Z.-Y. Yuan, Self-supported cobalt phosphide mesoporous nanorod arrays: a flexible and bifunctional electrode for highly active electrocatalytic water reduction and oxidation, *Adv. Funct. Mater.* 25 (2015) 7337–7347.
- [51] B. Zhang, Y.H. Lui, L. Zhou, X. Tang, S. Hu, An alkaline electro-activated Fe–Ni phosphide nanoparticle-stack array for high-performance oxygen evolution under alkaline and neutral conditions, *J. Mater. Chem. A* 5 (2017) 13329–13335.
- [52] E. Tronc, P. Belleville, J.P. Jolivet, J. Livage, Transformation of ferric hydroxide into spinel by iron(II) adsorption, *Langmuir* 8 (1992) 313–319.
- [53] G.K. Reddy, P. Boolchand, P.G. Smirniotis, Unexpected behavior of copper in modified ferrites during high temperature WGS reaction-aspects of $\text{Fe}^{3+} \leftrightarrow \text{Fe}^{2+}$ redox chemistry from Mössbauer and XPS studies, *J. Phys. Chem. C* 116 (2012) 11019–11031.
- [54] S. Boyanov, J. Bernardi, F. Gillot, L. Dupont, M. Womes, J.M. Tarascon, L. Monconduit, M.L. Doublet, FeP: another attractive anode for the Li-ion battery enlisting a reversible two-step insertion/conversion process, *Chem. Mater.* 18 (2006) 3531–3538.
- [55] K. Hirosea, T. Honmaa, Y. Doib, Y. Hinatsub, T. Komatsua, Mössbauer analysis of Fe ion state in lithium iron phosphate glasses and their glass-ceramics with olivine-type LiFePO_4 crystals, *Solid State Comm.* 146 (2008) 273–277.
- [56] E.M. Coe, L.H. Bowen, R.D. Bereman, A Mössbauer and X-ray powder diffraction study of some ferrous hematines, *J. Inorg. Biochem.* 58 (1995) 291–296.
- [57] J. Jacob, M.A. Khadar, VSM and Mossbauer study of nanostructured hematite, *J. Magn. Magn. Mater.* 322 (2010) 614–621.